Journal of Power Sources 285 (2015) 16–28

Contents lists available at ScienceDirect

Journal of Power Sources

journal homepage: www.elsevier.com/locate/jpowsour

Creep properties of catalyst coated membranes for polymer electrolyte fuel cells

Alireza Sadeghi Alavijeh, Ramin M.H. Khorasany, Aronne Habisch, G. Gary Wang, Erik Kjeang*

School of Mechatronic Systems Engineering, Simon Fraser University, 250-13450 102 Avenue, Surrey, BC V3T 0A3, Canada

HIGHLIGHTS

- Creep properties of catalyst coated membranes were compared to pure membranes.
- CCM creep was strongly influenced by the applied stress and hygro-thermal conditions.
- Catalyst layer microcracks were formed at the yield point of the CCM.
- Accumulation of creep damage was observed during successive creep-recovery steps.

GRAPHICAL ABSTRACT

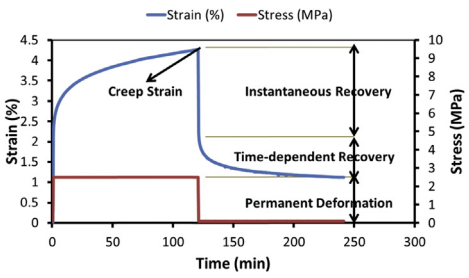

ARTICLE INFO

Article history:
Received 31 December 2014
Received in revised form
6 February 2015
Accepted 12 March 2015
Available online 14 March 2015

Keywords:
Fuel cell
Catalyst coated membrane
Creep
Recovery
Damage

ABSTRACT

Creep as a time-dependent mechanical damage acting either independently or in conjunction with other degradation mechanisms is known to reduce the membrane durability of polymer electrolyte fuel cells (PEFCs). Due to the important ionomer coupling of membrane and catalyst layers in PEFCs, the present work evaluates membrane creep when constrained within a catalyst coated membrane (CCM). Three key factors dominating creep life in commonly used perfluorosulfonic acid (PFSA) ionomer membranes, including creep stress, temperature, and relative humidity, were investigated by applying *ex-situ* creep loading and unloading experiments under controlled temperature and humidity conditions. The creep strain and recovery of the CCM were found to be highly dependent on the environmental conditions and applied stress levels, where the temperature effect on creep strain was the most significant. Repetitive creep – recovery cycles revealed that significant creep damage can accumulate in the material over time. This accumulated creep damage was found to be independent of the loading frequency while both peak strain and permanent deformation increased with the stress duration. Based on the present findings, it is recommended to reduce the operating temperature and ensure adequate membrane hydration in order to mitigate harmful creep effects in PEFCs.

1. Introduction

Polymer Electrolyte Fuel Cells (PEFCs) are a promising alternative to combustion engines in automotive applications. One of the main challenges facing the commercialization of PEFCs is in the development of membrane electrode assemblies (MEAs) that meet automotive industry durability targets [1] that range from 5000 h for light duty vehicles (e.g., passenger cars) to 18,000 h for heavy duty vehicles (e.g., transit buses) [2,3]. Currently, perfluorosulfonic acid (PFSA) ionomer membranes (e.g. Nafion® from DuPont) are the most commonly used membrane type in PEFCs due to the high

* Corresponding author.
E-mail address: ekjeang@sfu.ca (E. Kjeang).

http://dx.doi.org/10.1016/j.jpowsour.2015.03.082
0378-7753/

chemical stability inherited from the polytetrafluoroethylene (PTFE) structure [1,4]. Ionomer membranes are subjected to chemical and mechanical degradation during fuel cell operation [1,5–10]. The destructive effect of each mechanism (chemical and mechanical) is intensified in the presence of the other, and the final failure is often a combination of different degradation mechanisms [1]. Chemical degradation is caused by the attack of hydroxyl (•OH) and hydroperoxyl (•OOH) radicals primarily formed from hydrogen peroxide under the severe chemically oxidizing and reducing environment inside the fuel cell [1,5,7]. Mechanical degradation, on the other hand, is a result of mechanical stresses in the form of creep and hygrothermal fatigue, induced by temperature and humidity variations.

In order to improve the fuel cell performance and minimize ohmic losses, it is desirable to reduce the thickness of the membrane. Hence, developing mechanically durable membranes capable of maintaining structural integrity under various duty cycles is a critical target. The mechanical properties of PFSA membranes [8,9,11–13] are sensitive to variations in temperature and relative humidity. The effect of environmental conditions on the Young's modulus and yield stress of Nafion® 112 was reported by Tang et al. [11] via tensile tests at different temperature and humidity conditions, indicating a reverse relationship between the applied environmental conditions and the membrane tensile properties [11]. Similar mechanical properties were obtained by Bauer et al. [9] and Kundu et al. [12] for Nafion® 117. Bauer et al. [9] expressed an interaction between the temperature and humidity effects and suggested that water acts as a plasticizer at low temperatures and as a stiffener at high temperatures [9]. The tensile properties of PFSA membranes and catalyst coated membranes (CCMs) were recently evaluated, compared, and modeled by our group [14,15]. Under a wide range of environmental conditions, the CCM exhibited lower yield stress, yield strain, and Young's modulus when compared to the corresponding pure membrane. In both materials, the yield stress and Young's modulus decreased with increasing temperature and/or relative humidity, while the humidity induced expansion/contraction of the CCM were significantly suppressed compared to the pure membrane [14]. Furthermore, the peak and residual stresses during dehydration of the membrane were reduced in the presence of catalyst layers [16]. Due to the significant ionomer phase interaction between the membrane and catalyst layers in the CCM, it was recommended to treat the CCM as an independent composite material [14].

Creep in general is defined as time dependent deformation under constant applied stress in a material [17]. Under fuel cell operating conditions, this time dependent elongation could be detrimental and finally causes catastrophic failures due to hydrogen leaks or electrical shorts. To reach failure under creep stress, long periods of loading are required which may vary from a few hours to a few hundreds of years depending on the type of material and conditions [17]. Therefore, stress rupture tests have been introduced in order to estimate the creep lifetime [18]. Rupture tests are conducted under high levels of stress and temperature in order to accelerate the creep damage, and the results are extrapolated to predict the lifetime under the expected conditions [18]. As a thermally activated process, creep mechanisms are intensified exponentially with elevated temperature [18], but can also occur at room temperature in certain materials with low melting temperature, e.g. polymers. In addition to the temperature, creep strain is a function of the applied stress, time [18], and humidity [19,20]. In polymers, once the applied stress is released, a certain portion of the creep strain is recovered instantaneously followed by a gradual strain recovery due to the visco-elastic − visco-plastic nature of the material. Creep strain may also remain in the polymer as permanent deformation. Maksimov et al. [19] examined the creep properties of polyester below yield stress and showed that analogous to temperature, elevated humidity would increase the creep compliance [19]. Scaffaro et al. [20] measured the creep behavior of Polyamide 6 under controlled environmental conditions. By increasing the humidity from 15% to 50%, they observed an increase in the initial creep rate although the final strain was similar [20]. They expressed that at 50% RH, in the early stages humidity acts as a plasticizer and facilitates chain slip in the amorphous phase. However, the increase in crystallinity due to the structural rearrangement caused by creep strain slows down the creep rate [20]. Launay et al. [21] modeled non-linear mechanical response of cyclic creep and recovery in a polymer matrix composite of polyamide. They proposed an equivalence principle between the temperature and humidity validated by obtaining similar behavior at 70 °C–72% RH and 90 °C–50% RH [21]. In addition to conventional creep and creep rupture tests, Tweedie and Van Vliet [22] studied the creep behavior of different visco-elastic polymers using nanoindentation as a function of maximum creep force, force rate, and stylus geometry. A similar approach was utilized by Lu et al. [23] to study the linear visco-elastic properties of polymethyl methacrylate (PMMA) and polycarbonate (PC). Based on the time-temperature superposition principle, Achereiner et al. [24] investigated the long-term creep behavior of polypropylene via accelerated testing by elevating the temperature in brief steps. By rescaling the results of short-term tests, master curves for long-term creep capable to predict polypropylene creep response at different times were summarized [24].

PFSA ionomer membranes as visco-elastic − visco-plastic materials encompass viscous characteristics [17,25]. Under constant stress, the typical response of a viscous polymer includes an instantaneous increase in strain due to the elastic–plastic response followed by continuous straining at a non-constant rate due to the mixed elastic–plastic and viscous effects [17,26,27]. This continuous straining under constant stress is defined as creep. The polymer will continue to deform slowly with time until rupture. As the stress is released, an immediate strain recovery occurs followed by a gradual strain recovery. In most cases some strain is not completely recovered and remains permanently inside the membrane after stress removal [17]. Creep damage in PFSA membranes may either cause crack initiation or reduction in the membrane thickness until the membrane fails to separate the reactant gases [28]. Majsztrik et al. [29] investigated the influence of temperature and hydration on tensile creep in Nafion® N1110 and realized that the creep strain is greatly affected by both factors. At constant humidity, an increase in temperature always leads to higher creep strains while the impact of relative humidity varies depending on the test temperature [29]. At temperatures below 40 °C, high humidity resulted in low creep resistance due to the plasticizing effect of water, while at high temperatures above 90 °C, high humidity resulted in high creep resistance due to the adverse stiffening effect [29]. In the medium temperature range (40 °C < T < 90 °C) the creep resistance was highest at intermediate humidity due to the mutual effect of the aforementioned mechanisms [29]. From the same group, Satterfield et al. [30] compared the creep behavior of Nafion® 115 and Titania/Nafion® composite and expressed that lower creep strain was observed in the composite membrane. Creep failure of Nafion® NR111 was examined under various hydration and temperature levels by Solasi et al. [28]. The slope of the stress–rupture curves with respect to the time to failure was found to be independent of temperature and humidity in the applicable range. Through conducting cyclic and static biaxial blister tests, Li et al. [31] investigated the resistance to gas leakage in three different commercially available membranes under fatigue and creep loading. Due to the relatively identical creep and fatigue behavior at 90 °C and 2% RH, the lifetime was dominated by the

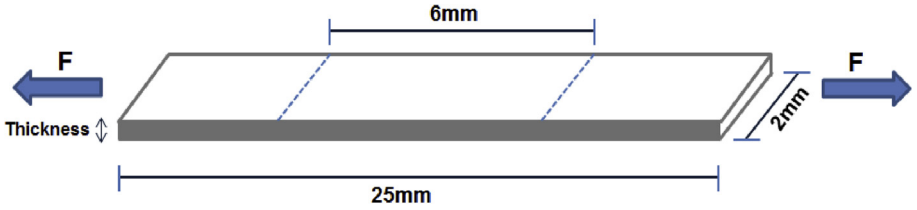

Fig. 1. Schematic of the rectangular sample used in creep testing (not to scale).

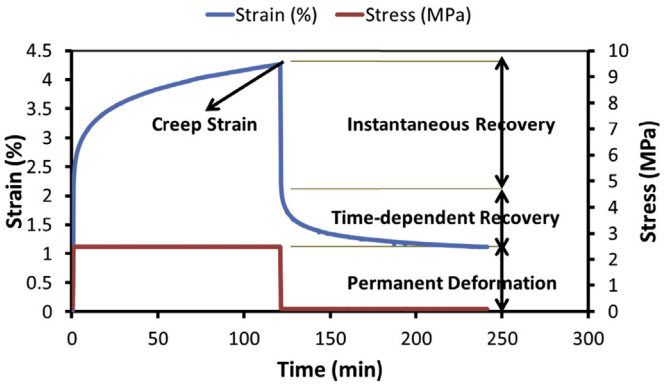

Fig. 2. Schematic of creep stress and strain profiles as a function of time applied on the membrane and CCM samples. Key metrics of the creep strain curve are illustrated.

total loading time rather than the number of cycles [31].

Despite the important ionomer phase coupling of membrane and catalyst layers in PEFCs, no previously published studies have considered membrane creep when constrained within a CCM. As reported previously by our group [14], membrane mechanical properties are significantly altered when coated by catalyst layers. Therefore, the objective of the present work is to thoroughly characterize the *ex-situ* creep response of catalyst coated PFSA membranes compared to pure membranes subjected to a variety of hygrothermal and mechanical stress conditions. Furthermore, accumulation of creep strains during conditions representative of dynamic PEFC operation will be evaluated through a series of successive creep stress and recovery cycles. In conjunction with our previous report on the static properties of CCMs [14], the outcomes of this work will provide complementary fundamental understanding of the dynamic behavior of CCMs in PEFCs.

2. Experimental procedure

2.1. Sample preparation

PFSA membranes and MEAs used for this study were provided by Ballard Power Systems. MEAs were prepared by coating a carbon supported platinum catalyst layer with PFSA ionomer on microporous layer (MPL) covered gas diffusion layer (GDL) to fabricate gas diffusion electrodes (GDE). Then, anode and cathode GDEs were hot pressed with a PFSA membrane to form the MEA. In order to prepare creep samples, PFSA membranes and MEAs were all cut into rectangular shapes (25 × 2 mm) along the transverse (cross-machine) direction. Then, GDLs were detached from both sides of the MEA and the remaining CCM and PFSA membrane samples were stored between glass slides in ambient conditions prior to creep testing.

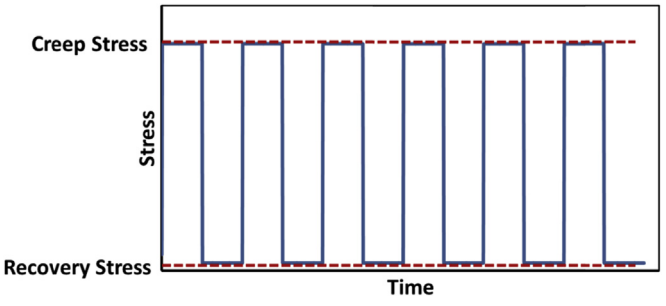

Fig. 3. Schematic of successive creep and recovery stresses applied on CCM samples. Stress values were selected depending on the yield strength of the material at the desired temperature and relative humidity.

2.2. Creep testing

Tensile creep tests were applied at various levels of controlled temperature, relative humidity, and stress on PFSA membrane and CCM samples using a dynamic mechanical analyzer (DMA; TA Instruments Q800) equipped with an environmental chamber (TA Instruments DMA-RH Accessory). Samples of 25 mm length were loaded at 6 mm initial gauge length and the remaining 19 mm length was used to clamp the sample. The exact gauge length and sample width were measured for all samples by the DMA and optical microscope, respectively, while the average thickness was quantified by digital micrometer prior to the test at ambient conditions. Approximate sample dimensions are illustrated in Fig. 1, schematically.

As explained before, creep testing requires long periods of loading to reach sample failure due to the slow propagation of creep damage. Therefore, in this study, creep experiments were

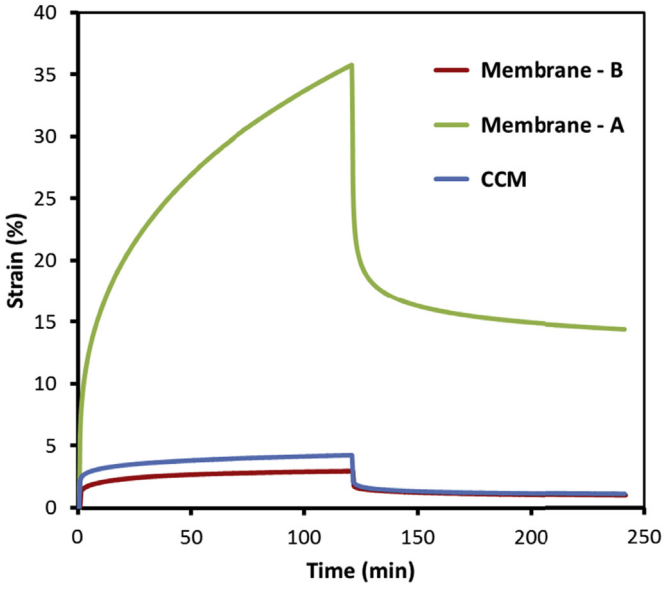

Fig. 4. Strain – time curves of the CCM, membrane-A (identical load), and membrane-B (identical stress) at 23 °C–50% RH.

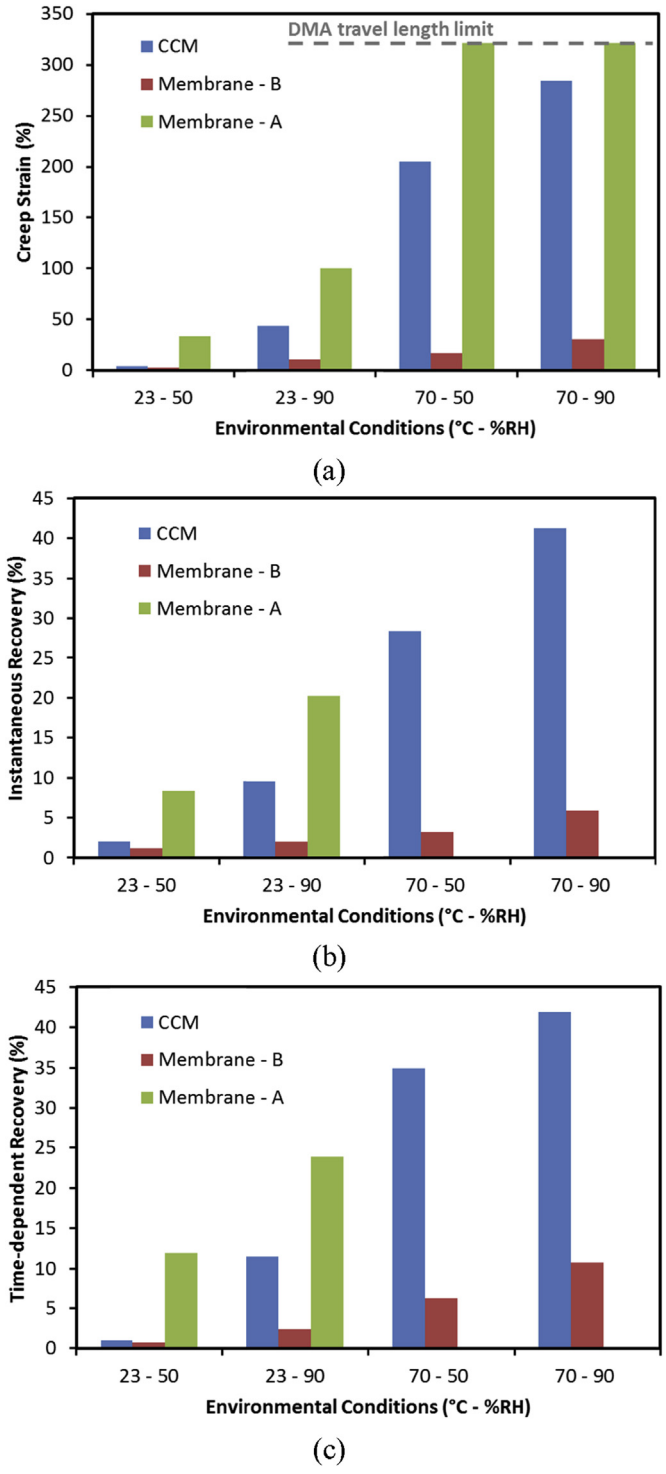

Fig. 5. Measured creep properties of a CCM compared to a pure membrane at different hygrothermal conditions. Membrane-A and membrane-B were subjected to the same load and stress as the CCM, respectively.

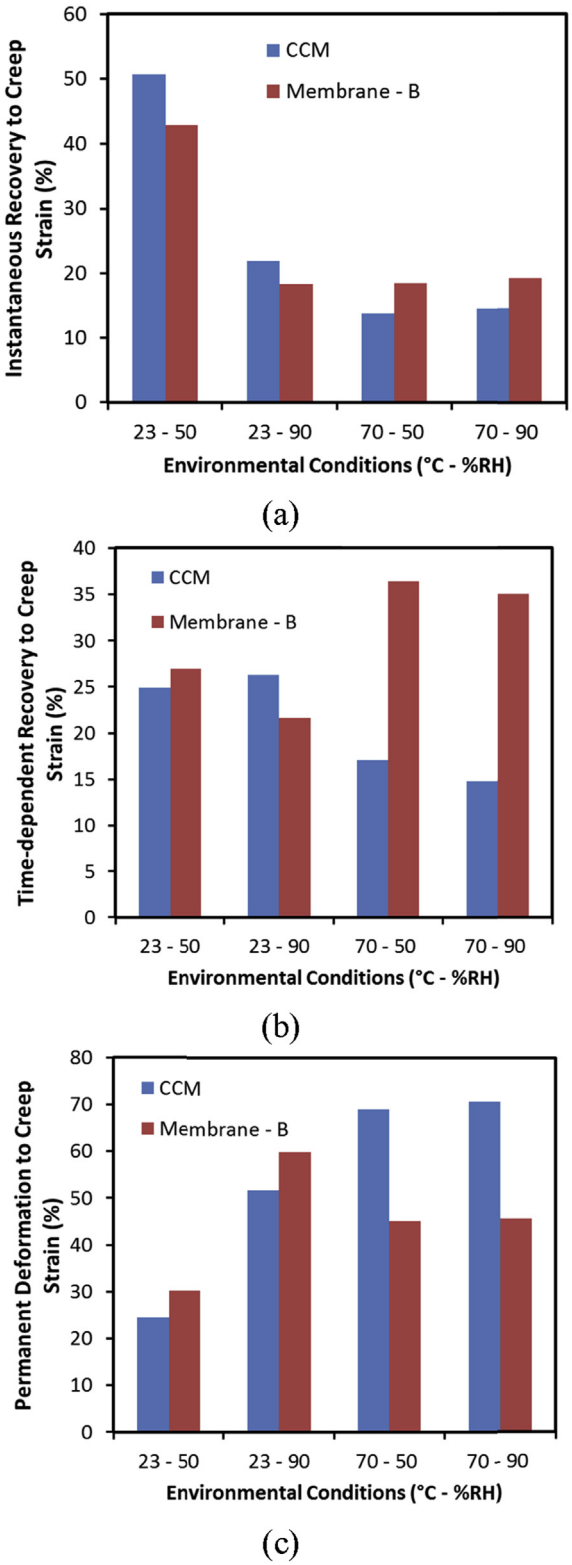

Fig. 6. Ratio of (a) instantaneous recovery, (b) time-dependent recovery, and (c) permanent deformation to the total creep strain in the CCM and membrane-B (identical stress) samples at different hygrothermal conditions.

designed to measure the creep and recovery response in a reduced time period of a few hours, which is deemed sufficient for fuel cell applications [29]. Prior to creep test initiation, the samples were loaded at ambient conditions and equilibrated to the desired temperature and relative humidity conditions while a small pre-load tensile stress (0.1 MPa) was applied to keep the sample under tension. In order to avoid shocking the samples with a jump in stress, the creep stress was elevated to the predetermined stress at a relatively high rate (5 MPa min^{-1}). With the aim of assessing the effects of hygrothermal conditions, stress, and time on the creep response of the materials, three types of creep experiments were conducted:

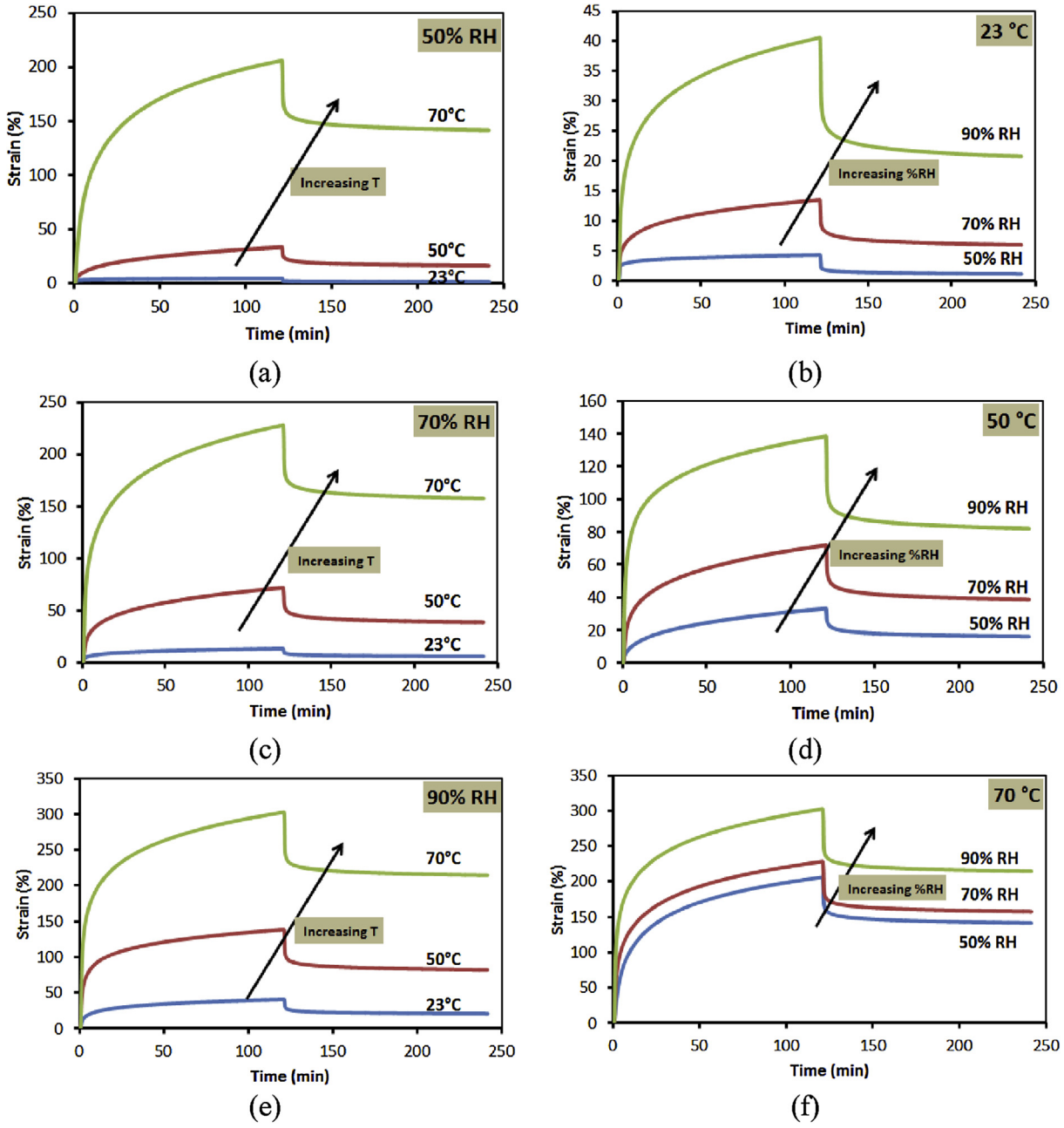

Fig. 7. Strain – time curves for CCM samples at different temperatures (23, 50, and 70 °C) and relative humidity (50, 70, and 90% RH) under 2.5 MPa creep stress.

1. Constant stress tests: With the purpose of understanding the effect of hygrothermal conditions on the creep behavior, regular creep tests were applied on the PFSA membranes and CCMs at different temperatures (23 and 70 °C) and relative humidities (50% and 90%). The creep properties of the CCM were compared to the membrane under equivalent stress (2.5 MPa) and equivalent force. Additional creep tests were performed on CCMs at intermediate temperature (50 °C) and relative humidity (70%) to provide more details on the impact of the environmental conditions on the creep response of the CCM. As depicted in Fig. 2, samples were stretched under constant creep stress for 120 min followed by 120 min of unloading to evaluate the *creep strain*, *instantaneous* and *time-dependent* factors of recovery, and *permanent deformation*. Creep strain represents the strain at the end of the loading step, while instantaneous recovery and time-dependent recovery indicate the strain restoration during stress reduction and during the recovery, respectively. Finally, permanent deformation shows the total unrecovered strain stored inside the membrane. As explained, applying a small tensile stress value (0.1 MPa) during the unloading was mandatory in order to keep the samples straight during the test. Each of the aforementioned tests was repeated at least two times according to the ASTM D2990 creep standard [32] and the average creep strains were reported.
2. Variable stress tests: A similar procedure was applied to measure the creep deformation of CCMs as a function of creep stress at four combinations of temperature and relative humidity (23°C-50%, 23°C-90%, 70°C-50%, and 70°C-90%). The stress values were selected to be 40%, 60%, 80%, 100%, 120%, and 140% of the yield strength of the CCM at the desired test conditions as

Table 1
ANOVA of creep strain in CCM as a function of temperature and relative humidity under 2.5 MPa creep stress.

Factor	Creep strain		Permanent deformation	
	Effect (%)	P Value	Effect (%)	P Value
Temperature	220.6	<0.0001	159.5	<0.0001
Relative Humidity	59.6	<0.0032	40.7	<0.0039
Interaction	19.9	<0.1020	19.0	<0.0493

previously reported by Goulet et al. [14]. In the same manner, the average of at least two tests was reported for each testing conditions [32].

3. Fuel cell simulated (FCS) tests: Under automotive operating conditions, the membrane is subjected to cycles of hygrothermal loading and unloading in addition to the static mechanical compression of the MEA. Understanding the accumulation of creep damage was accomplished through applying successive steps of creep and recovery at room and fuel cell conditions (23°C-50%RH and 70°C-90%RH, respectively), as presented in Fig. 3. Fuel cell simulated tests were repeated three times at each test parameter as per the ASTM D2990 requirements [32].

2.3. Microstructural analysis

Top surface microstructural analysis of the CCM samples after being subjected to the variable stress creep experiments was performed using scanning electron microscopy (SEM; FEI Dualbeam 235 FIB-SEM) at Simon Fraser University's nano-imaging facilities at 4D LABS. SEM images were captured from the gauge section of the creep samples using 5 kV electron beam accelerating voltage.

3. Results and discussion

The creep properties of catalyst coated PFSA membranes (CCMs) were systematically evaluated and compared to pure membranes using *ex-situ* tensile creep tests. First, the creep behavior of CCMs was analyzed under various levels of temperature and relative humidity. Then, the effect of creep stress on the creep strain and recovery was evaluated. Finally, the accumulation of creep deformation during simulated fuel cell operating conditions was investigated under cyclic periods of loading and unloading.

3.1. Constant stress tests

The physical and mechanical properties of PFSA membranes in PEFCs are highly sensitive to the environmental conditions, primarily due to the hygroscopic nature of the ionomer material. In automotive PEFCs, an MEA is subjected to signification variations in temperature and relative humidity, for instance from ambient conditions (e.g., 23 °C and 50% RH) to fuel cell operating conditions (e.g., 70 °C and 90% RH) during startup, which may lead to membrane creep and subsequent damage. As explained in the experimental procedure, two types of constant stress creep tests were conducted in order to evaluate and compare the CCM creep behavior to that of a pure PFSA membrane. In addition, the anticipated reinforcing effect of the catalyst layers on the CCM creep resistance was examined. The two types of creep tests performed on the reference membrane samples were CCM identical force (membrane - A) and CCM identical stress (membrane - B). Strain – time curves for the CCM and membranes subjected to creep at 23 °C–50% RH are shown in Fig. 4. In addition, the total creep and recovery data extracted from the strain – time curves at various environmental conditions are illustrated in the bar charts of Fig. 5. As expected, the creep strain and recovery was higher

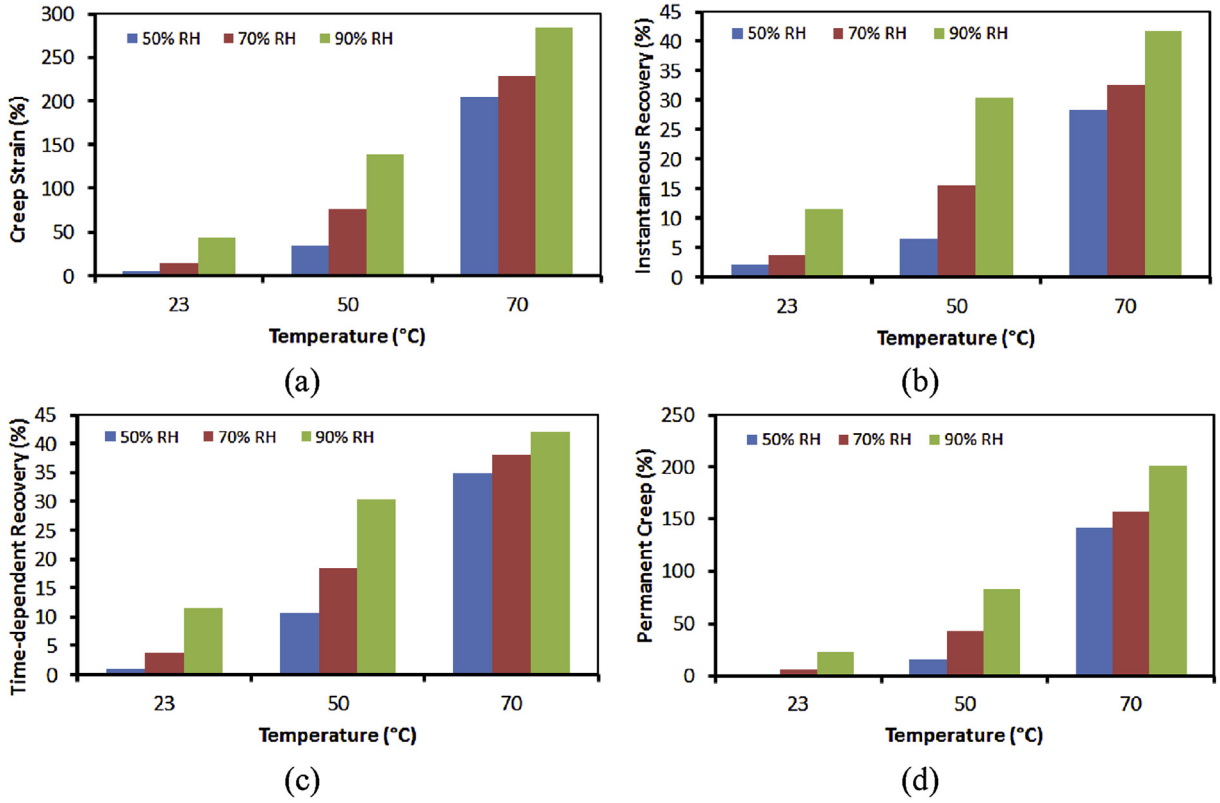

Fig. 8. (a) Total creep strain, (b) instantaneous creep recovery, (c) time-dependent creep recovery, and (d) permanent creep deformation in the CCM as a function of temperature and relative humidity under 2.5 MPa creep stress.

Table 2
Summary of the CCM yield strength measured by Goulet et al. [14], using the same CCM material as in the present study.

Temperature (°C)	Relative humidity (%)	Yield strength (MPa)
23	50	3.7
70	50	2.0
23	90	2.3
70	90	1.1

in membrane-A than for membrane-B due to the higher applied force (and stress). Approximately three times higher stress was applied on membrane-A, resulting in approximately ten times higher creep strain. At identical force (CCM and membrane-A), the creep strain of the CCM was remarkably lower than that of the membrane, indicating the reinforcement provided by the catalyst layers. It can be summarized that the catalyst layers improved the membrane resistance to creep deformation independent of the environmental

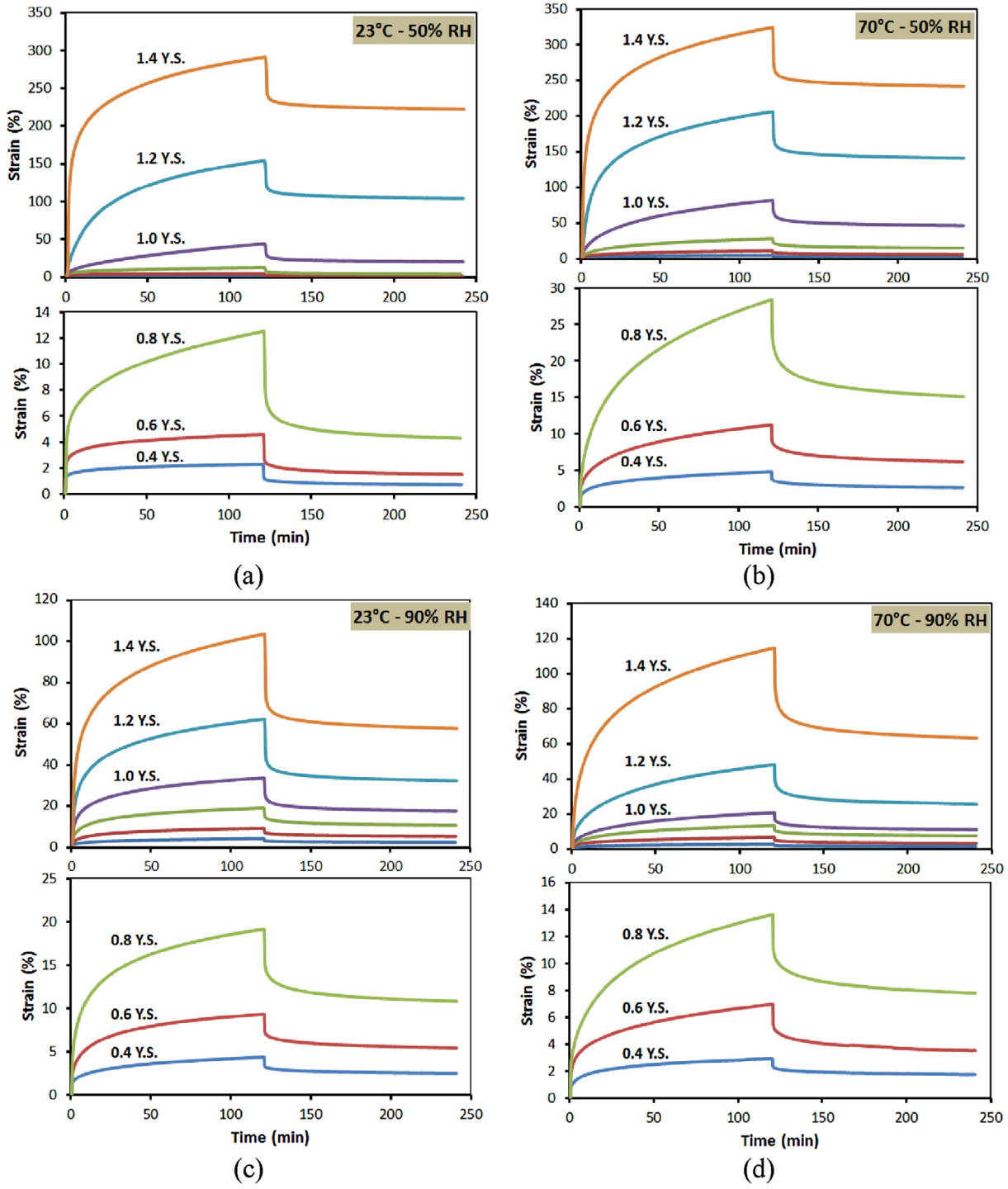

Fig. 9. CCM creep strain curves at different levels of stress at four combinations of temperature and relative humidity. The stress is indicated relative to the yield stress (Y.S.) under each environmental condition. Due to the large variations in strain under different stress levels, the low stress curves were magnified and reproduced in a separate window below each corresponding plot.

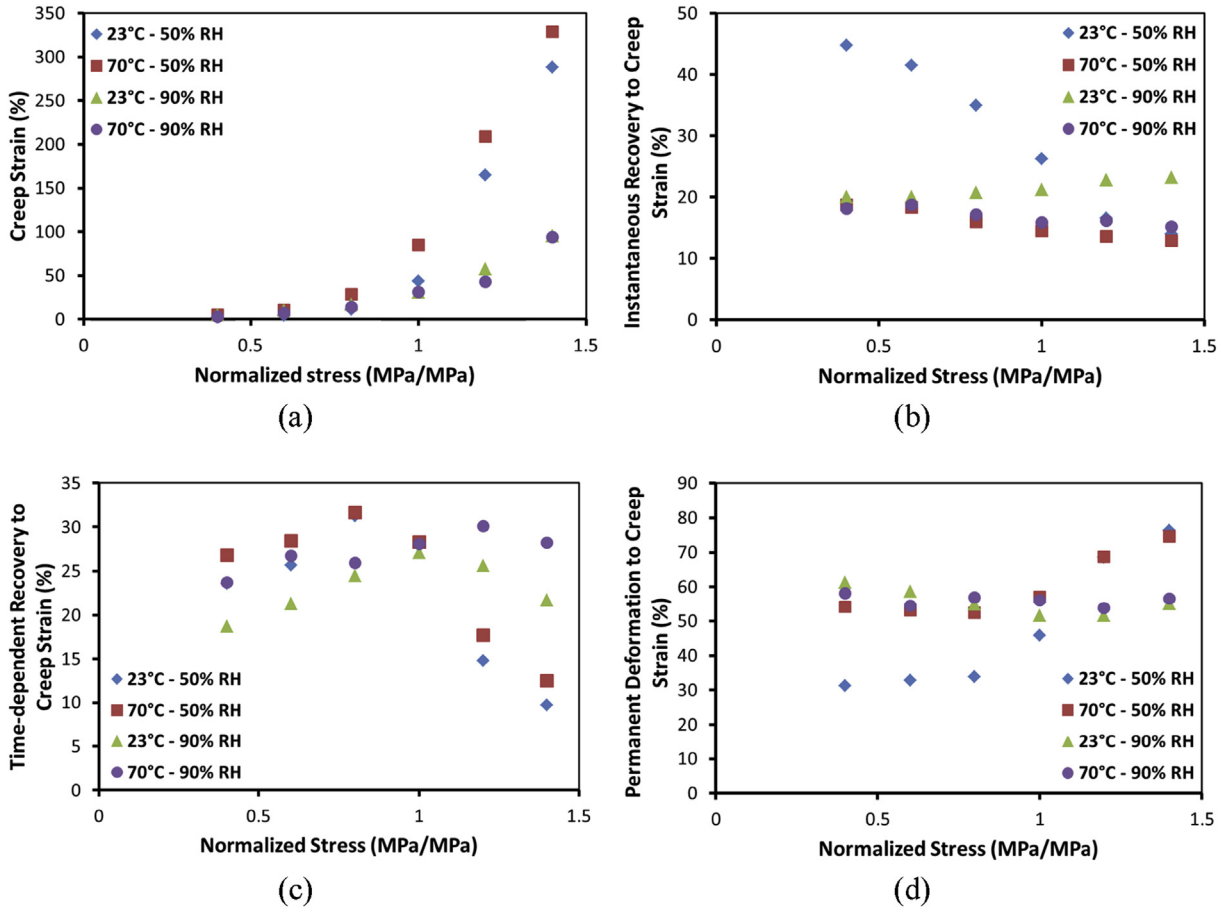

Fig. 10. CCM creep strain results at various levels of applied stress (normalized by the yield stress at each environmental condition). (a) Total creep strain and ratio of (b) instantaneous recovery, (c) time-dependent recovery, and (d) permanent deformation to the total creep strain.

conditions, as the creep strain was reduced by 88% and 56% at 23 °C–50% RH and 23 °C–90% RH, respectively. In a similar manner, the total strain recovery (instantaneous and time-dependent) was reduced by 85% and 52% respectively. It should be mentioned that at 70 °C–50% RH and 70 °C–90% RH, the membrane-A tests were terminated due to the relatively large creep strains approaching the DMA travel length limit (~26 mm); hence, no recovery data were measured in these cases. On the other hand, at identical stress (CCM and membrane-B), the CCM exhibited higher creep strain than the membrane at all environmental conditions, which revealed a lower creep resistance in the catalyst layers compared to the membrane. The porous structure accompanied with the fragile bonding among particles limit the mechanical strength of the catalyst layers [14]. For this reason, the membrane is the main load bearing part of the CCM.

The ratio of creep recovery and permanent deformation to the total creep strain in the CCM and membrane-B (identical stress) are presented in Fig. 6. At low temperature, the portions of recovery and permanent deformation were relatively identical for the two materials, although the permanent deformation ratio increased with humidity. However, the aforementioned ratios were substantially altered as the temperature increased, where the permanent deformation of the CCM was considerably higher than for the membrane due to a lack of time-dependent recovery. According to our previous study [14], the applied 2.5 MPa creep stress was beyond the CCM yield point at high temperature (70 °C) while it was well below the membrane yield point. Therefore, due to the viscoplastic deformation of the CCM compared to the mainly viscoelastic deformation of membrane-B under 2.5 MPa creep stress, smaller portions of the creep strains were reclaimed during the time-dependent recovery of the CCM compared to the membrane.

A supplementary study on the effect of hygrothermal conditions on the creep behavior of the CCM was conducted by measuring the creep and recovery at an intermediate temperature (50 °C) and relative humidity (70%) following the constant stress creep test. Fig. 7 shows the CCM creep strain curves as a function of temperature and relative humidity. It is evident from Fig. 7 that an increase in temperature or relative humidity always results in higher creep strain and deformation. Creep occurs when sufficient driving force is provided by the applied stress to overcome the molecular interactions of the polymer. The requisite driving force decreases exponentially as temperature increases due to the thermally activated nature of creep in polymers [28]. Therefore, Arrhenius type equations are suggested to express the exponential contribution of temperature and humidity on the creep strain rate [28]. F-test analysis of variance (ANOVA) was applied to quantitatively study the effects of the environmental conditions using the lowest and highest temperature and relative humidity values. According to the ANOVA outcomes summarized in Table 1, it appears that the influence of temperature on the creep strain and permanent deformation is more significant than the impact of relative humidity while the interaction has the lowest effect when compared to each individual parameter. Based on the p values in Table 1, at a significance level of 0.01, the effects of temperature and relative humidity are both statistically significant while the interaction effect is not. As the temperature increases, the internal energy of the membrane

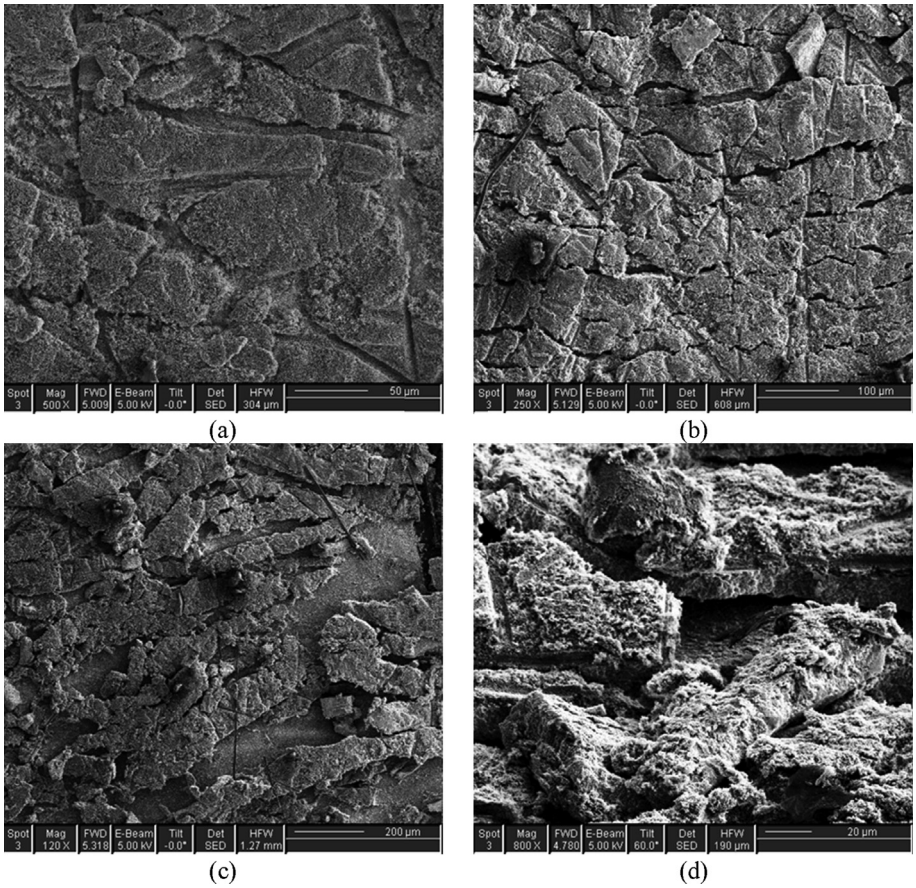

Fig. 11. Surface SEM images of crack formation in the cathode catalyst layer during CCM creep testing at 70 °C–90%RH. The images show the cathode surface of (a) a pristine CCM before creep testing, (b) a post-creep CCM subjected to yield stress, and (c, d) a post-creep CCM subjected to 140% of the yield stress (shown at 0° and 60° tilt from the normal direction, respectively). The creep stress was applied in the vertical direction of the images.

enhances the motion of molecules and the relative slip of adjacent chains, resulting in higher elongation under creep stress. In contrast, relative humidity facilitates creep deformation through swelling and distancing the molecular chains.

The impact of the coupled hygrothermal conditions on the individual steps of creep and recovery in the CCM is exhibited in Fig. 8. The effect of relative humidity on the creep strain and recovery was more significant at low temperatures (e.g. 23 °C) than at high temperatures (e.g. 70 °C). As an example, the total creep strain at 23 °C (Fig. 8a) increased by nearly eleven times when the RH was raised from 50% to 90%, while at 70 °C (Fig. 8a), the total creep strain increased by merely 40%. Nafion® membrane creep responses at lower humidities than the ones addressed in our study on CCMs were reported by Majsztrik et al. [29]. Their results on the humidified membranes (8% and 65% RH) at temperatures below 70 °C are qualitatively in agreement with our findings for the CCM [29]. However, a completely different behavior was observed in fully dried (0% RH) membranes where the creep strain above 50 °C was higher than for the humidified membranes (8% and 65% RH). At low temperatures, the water absorbed in the ionomer acts as a plasticizer and enhances the slip of polymer molecules; hence, increasing the humidity generally facilitates the flow of molecules. As the temperature is increased, due to the adequate thermal energy obtained by the molecular chains, molecular flow under the creep stress is facilitated. Thus, the plasticizing effect of relative humidity becomes less significant on the creep deformation.

Similar behavior was observed in the recovery stage (Fig. 8b–d) after the creep stress was released. It is noteworthy that the creep stress (2.5 MPa) applied in these experiments was in some cases higher than the yield stress of the CCM, as previously measured by our group [14] and exhibited in Table 2 at four temperature and relative humidity combinations. It can be seen from Fig. 8 that at high temperatures and relative humidities, where the yield point was passed, most of the creep strain was stored in the sample after the recovery and only minor portions were released during the recovery stage. In contrast, at conditions below the yield point, most of the creep strain was reclaimed during the recovery. For example, by comparing Fig. 8a with Fig. 8d, at 70 °C–90% RH, 71% of the creep strain remained inside the sample after recovery as permanent creep deformation. While at 23 °C–50% RH, only 27% of the creep strain remained as permanent creep deformation.

3.2. Variable stress tests

In this section, the effect of the creep stress on the CCM creep strain and recovery was investigated under fixed hygrothermal conditions by means of tensile creep measurements under different stress levels from 40% to 140% of the CCM yield stress [14]. Among the environmental conditions studied in the previous section, four combinations of temperature (23 and 70 °C) and relative humidity (50% and 90% RH) were considered here, with results shown in Fig. 9. Due to the large variations in strain at different stress levels, the strain curves related to low stress levels (40%, 60%, and 80% of the yield stress) were magnified and reproduced in an additional plot window. As expected, the higher stress magnitude resulted in

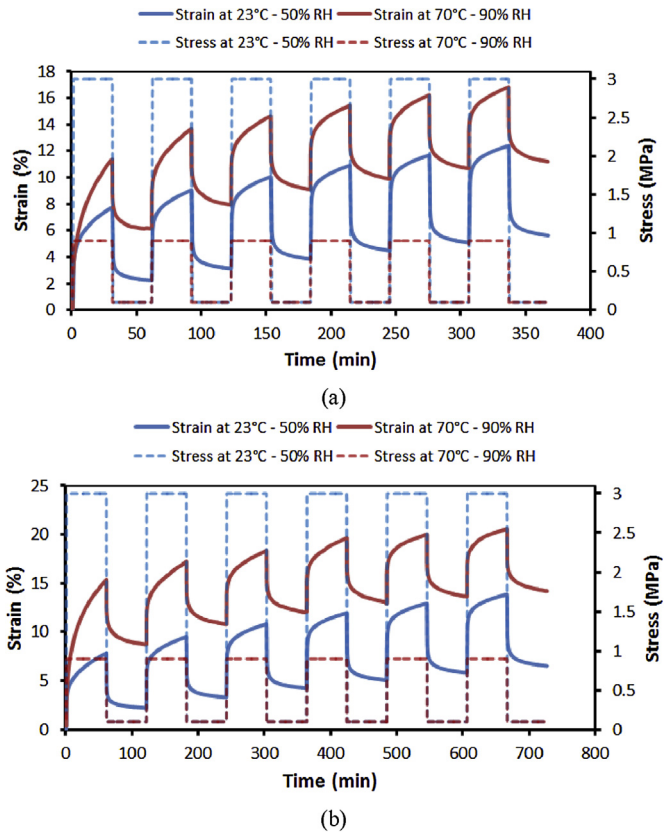

Fig. 12. Multi-step creep response of CCM samples at room and fuel cell conditions for (a) 30 min and (b) 60 min steps.

Table 3
Recovery and deformation relative to the total creep strain at the end of the multi-step creep tests.

Test conditions	Instantaneous recovery (%)	Time-dependent recovery (%)	Permanent deformation (%)
23 °C – 50% RH – 30 min	34.4	20.6	45.0
23 °C – 50% RH – 60 min	30.6	22.3	47.0
70 °C – 90% RH – 30 min	17.7	16.0	66.3
70 °C – 90% RH – 60 min	16.0	15.1	68.1

higher creep strain, independent of the environmental conditions. The most dramatic variation was observed at 23 °C–50% RH where the creep strain increased from 2.2% to 288% at 40% and 140% of the yield stress, respectively. At higher temperature and humidity, the rate of increase in creep strain due to stress elevation decreased (e.g., from 3.1% to 94% at 70 °C–90% RH) but still remained significant.

The total creep strain and various recovery portions were extracted from the creep strain curves and illustrated in Fig. 10 as a function of normalized stress. The normalized stress was calculated as the ratio of the applied creep stress to the yield stress at the corresponding temperature and relative humidity. As expected, the creep strain increased nonlinearly with an increasing slope as the stress was elevated. The instantaneous portion of recovery remained relatively constant in the 10–25% range under most conditions, except under room conditions (23 °C–50% RH) where a much higher degree of instantaneous recovery (up to 45%) was obtained for stress values below the yield point (Fig. 10b), indicative of a more elastic behavior. Creep deformation generally occurs due to the breakage of cross links between polymer molecules under creep loading. During recovery, the intermolecular bonds tend to re-entangle and reproduce the cross links. At high temperature and/or humidity, however, the molecular vibrational energy is high enough to decelerate the re-arrangement of lateral links shortly after stress removal. Therefore, the portion of instantaneous recovery of creep strain is small and varies negligibly with the creep load. In contrast, the low molecular vibrational energy at room conditions facilitates the re-arrangement of intermolecular forces quickly after release of stress, resulting in larger portions of instantaneous recovery.

On the other hand, the time-dependent strain recovery inherited from the partially viscous nature of the PFSA ionomer was found to reach a maximum level around the yield point for each hygrothermal condition (Fig. 10c), which is a consequence of the viscoelastic behavior below the yield stress compared to the viscoplastic behavior above the yield stress. The irreversible viscoplastic creep accompanied with strain hardening restricted the time-dependent recovery and enlarged the permanent deformation. Reorientation of the sulfonic acid groups in the hydrophilic clusters combined with the deformation of the PTFE matrix contribute to the time-dependent recovery [29]. Below the yield point, creep stress facilitates the reorientation of sulfonic acid groups resulting in an increasing regime in time-dependent recovery strain. However, beyond the yield point, due to the flow of polymer molecules, the relative contribution of time-dependent recovery is reduced and overshadowed by the permanent deformation.

Finally, significant permanent deformation of at least 30% of the total creep strain was observed under all conditions (Fig. 10d), even for applied stresses below the yield point. Interestingly, the relative permanent deformation at high humidity (90% RH) was almost constant at 50–60%, independent of the applied stress level, while at low humidity (50% RH) the relative permanent deformation was observed to increase past the yield point, as would normally be expected due to plastic deformation. At high RH, the plasticizer role of water is likely to reduce the sensitivity to stress, resulting in a constant fraction of permanent deformation. It should be noted that the two-hour creep recovery time used in the experiments was deemed sufficient in order to reach a relatively stable condition at which the permanent deformation could be reliably measured.

The microstructural evolution of the cathode catalyst layer portion of the CCMs subjected to different levels of creep stress at 70 °C–90%RH was investigated using scanning electron microscopy (SEM), with typical images shown in Fig. 11. The cathode catalyst layer was distributed uniformly on the membrane in the pristine CCM (Fig. 11a), with random indentations created by adjacent GDL fibers evident on the surface. Once the creep stress was applied, the membrane and catalyst layers were stretched accordingly. However, as deformation continued, the catalyst layers were not capable of elongating in the same manner as the membrane, due to the brittleness of the porous catalyst layer structure. Below the yield stress, the structural integrity of the pristine CCM was preserved during creep testing without resembling noticeable changes in the microstructure. At the yield stress, permanent microcracks were formed through the whole thickness of the cathode catalyst layer perpendicular to the stress direction (Fig. 11b). As the creep stress passed the yield point, islands of catalyst layer were formed on the surface of the membrane surrounded by interconnected macrocracks, as shown in Fig. 11c. Further microstructural analysis at 60° tilt revealed the detachment between catalyst layer and membrane, as illustrated in Fig. 11d. Membrane elongation is restricted in the presence of catalyst layers [14]. However, due to the large creep deformation beyond the yield point of the CCM and the relatively low ductility of the catalyst layers, the catalyst layers failed to

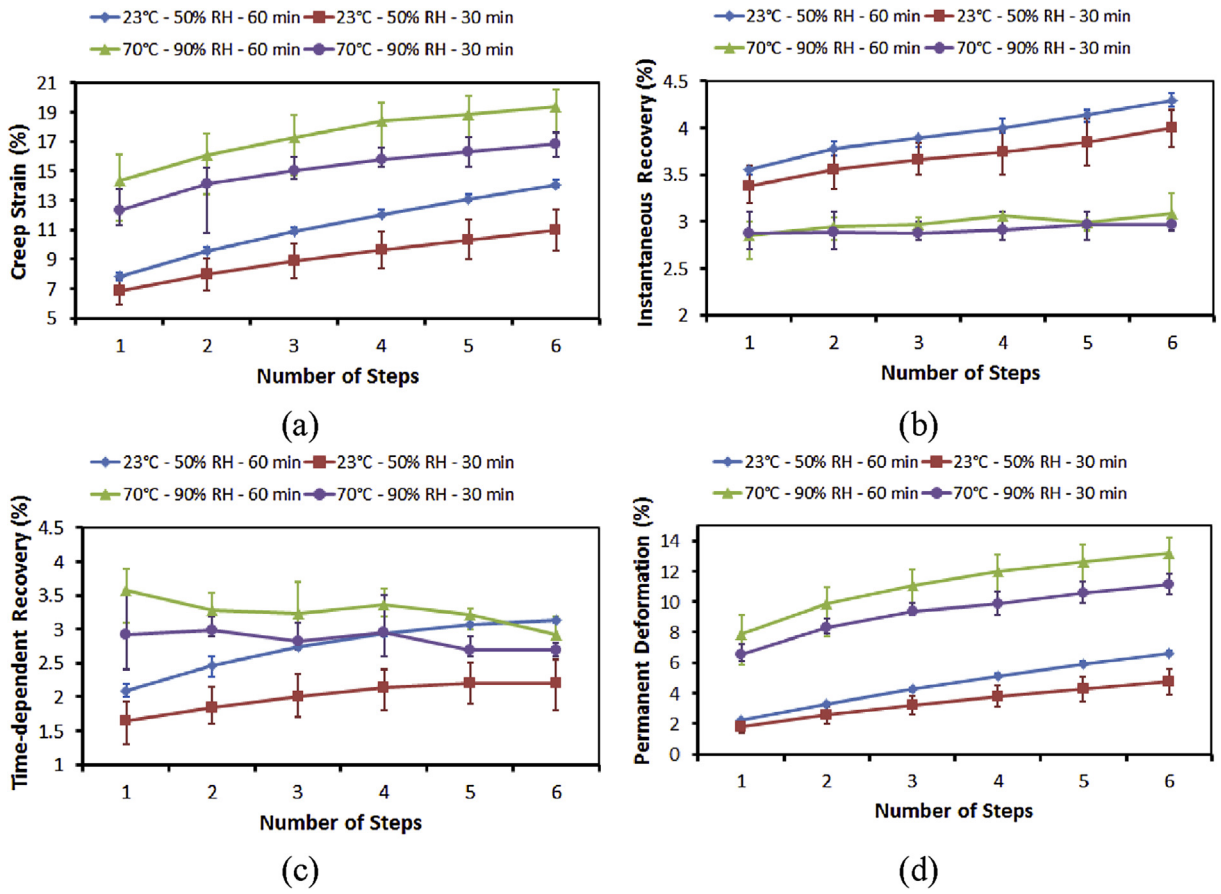

Fig. 13. Variations in (a) creep strain, (b) instantaneous recovery, (c) time-dependent recovery, and (d) permanent deformation in CCM samples with respect to the sequence of steps.

elongate in this regime. This resulted in the initiation and propagation of cracks in the cathode where the crack size increased with increasing level of stress past the yield point. The cathode failure and detachment is a further evidence of the rapid growth of creep strain beyond the yield point as presented in Fig. 10a. Here, membrane flow was readily facilitated because of the loss of reinforcement otherwise provided by the catalyst layers. Similar microstructures depicted in Fig. 11 were also observed at the other temperature and humidity conditions.

3.3. Creep under simulated fuel cell conditions

When situated inside an operating fuel cell, the CCM experiences significant dynamics due to startup/shutdown cycles and changes from low to high power that generate stress inside the material. The cyclic and static forces during operation impose fatigue and creep deformation in the membrane. As a result, portions of creep strain may remain inside the membrane, i.e., permanent deformation, and accumulate gradually until membrane failure. The sequence of working at high and low stresses can be simulated via successive steps of creep and recovery. Multi-step creep experiments were therefore conducted at room and fuel cell operating conditions (23 °C–50% RH and 70 °C–90% RH), and the resulting creep responses of the CCM are presented in Fig. 12. The creep stress was selected to be 80% of the CCM yield stress at the desired temperature and relative humidity. During recovery, a 0.1 MPa tensile stress was applied to keep the samples under tension. It can be seen that creep strain and permanent creep were accumulated gradually as the steps continued, with more significant deformation at fuel cell conditions than at room conditions. Ultimately, at room conditions, less than 50% of the creep strain was stored in the sample in the form of permanent deformation; while at fuel cell conditions, the permanent deformation was more than 65% of the creep strain, as presented in Table 3. As previously discussed, the high vibrational energy of the ionomer molecules at fuel cell conditions prevents the intermolecular cross links to be reconfigured during the recovery steps, resulting in larger permanent deformation when compared to room conditions. As presented in Fig. 6, the recovery of the membrane was limited in the presence of catalyst layers at high temperatures while the recovery portions of membrane-B were not affected by the temperature. It can be summarized that membrane-B would experience lower creep deformation at high temperatures when compared to CCM. In the same manner, higher fractions of strain were reclaimed during instantaneous recovery steps at room conditions when compared to fuel cell conditions (Table 3). This was due to the reconstruction of intermolecular bonds quickly after the stress relaxation at low temperature.

The accumulation of creep strains during the loading and unloading steps is further illustrated in Fig. 13 for the present combinations of step time and environmental conditions. From Fig. 13a, it is apparent that the creep strain increased almost linearly after the first step, with a higher rate at room conditions compared to fuel cell conditions. Furthermore, the creep curves corresponding to identical environmental conditions resembled higher creep strain in the CCMs subjected to creep loading and unloading for a longer time step (60 min as compared to 30 min).

At room conditions, the instantaneous and time-dependent

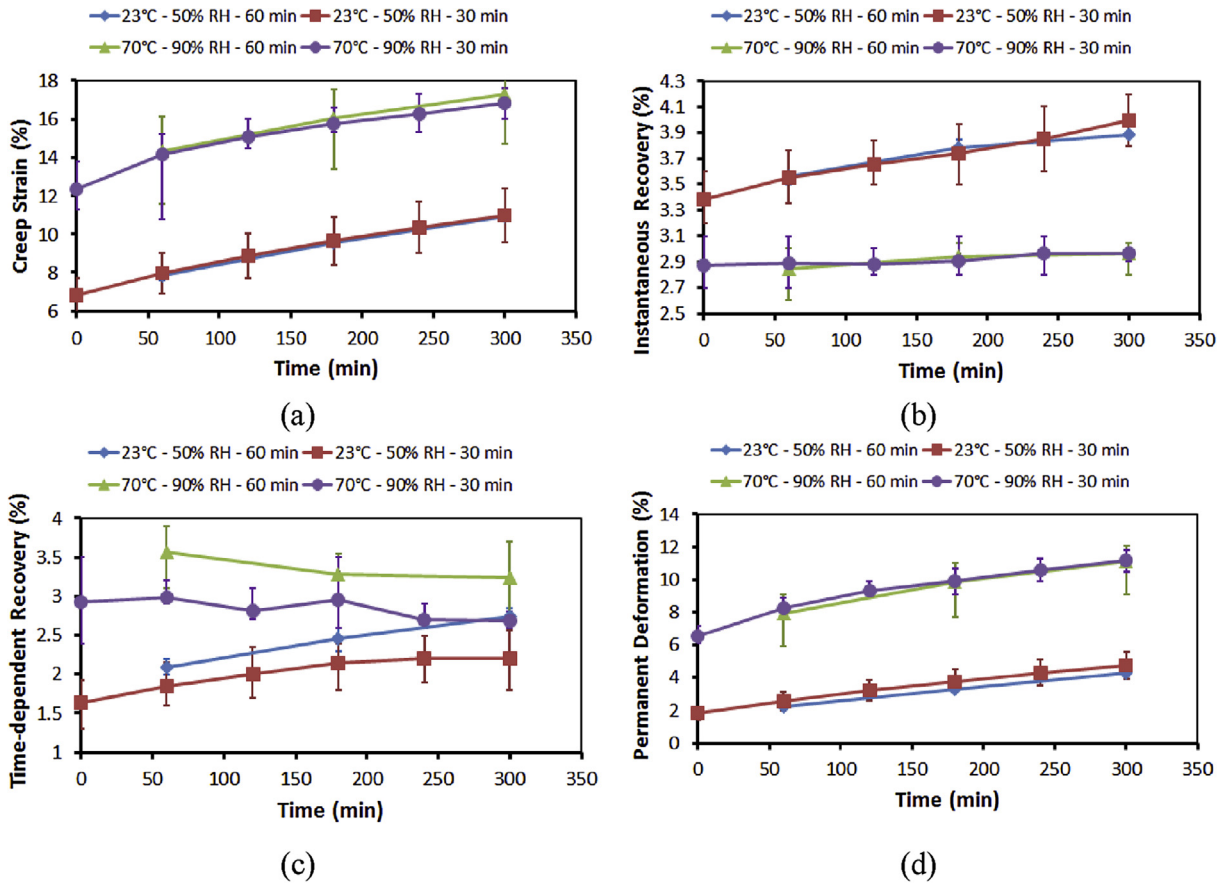

Fig. 14. Multi-step creep test results as a function of time: the first three 60-min steps of the low-frequency tests compared to all six 30-min steps of the high-frequency tests.

recovery strains increased as the test progressed. On the other hand, at fuel cell conditions, the magnitude of instantaneous and time-dependent recovery strains remained essentially constant after the first step. The constant recovery at fuel cell conditions shows that only certain amounts of creep strain can be restored elastically in each step and the rest of the creep strain accumulated during loading periods will be stored plastically. A comparison between the amount of strain released during recovery and the creep strain shows that larger portions of creep strain were released at room conditions compared to the fuel cell conditions. This, as explained before, is related to the facile reconstruction of cross links among molecules at room conditions due to the lower internal energy of polymer. Permanent deformation, according to Fig. 13d, increased similarly to the creep strain at both fuel cell and room conditions. It can be concluded that the creep damage accumulated gradually during each step and the magnitude of strain are related to the duration of the applied stress.

In order to reveal the role of the creep step frequency (time of each step), the curves in Fig. 13 are reproduced in Fig. 14 with respect to the test duration. In this figure, only the first three steps of each 60 min test are compared to all six steps of each 30 min test, where the CCMs experienced similar loading and unloading time in total. The curves corresponding to similar environmental conditions are observed to match very well except for the time-dependent recovery where slightly higher recovery was observed in the 60 min tests. In summary, at constant time and creep stress, the total creep strain is independent of the number of creep cycles, i.e., the frequency of the creep steps. In contrast, the dominating factor that controls the creep deformation is the total time that the sample endured the creep stress.

4. Conclusions

The creep behavior of catalyst coated membranes was evaluated through conducting tensile creep – recovery experiments as a function of temperature, relative humidity, and stress. It was observed that coating the membrane with catalyst layers strengthens the membrane resistance against creep deformation. Furthermore, the creep strain of the CCM was significantly promoted when the aforementioned variables were increased. Statistical analysis showed that temperature plays a greater role than humidity in the context of creep strain. The effect of stress on the creep response of CCM became more significant beyond the yield stress. Below the yield point, cross links can be re-entangled as the stress releases due to the lower internal energy of the membrane. Beyond the yield point, however, a longer time is required to retrieve the intermolecular bonds, not only because of the high internal energy of the membrane, but also due to the failure of the catalyst layers to reinforce the membrane. The mechanical support provided by the catalyst layers was only effective up to the yield point, at which permanent catalyst layer cracks were generated perpendicularly to the principal direction of the stress. Accumulation of creep damage during the multi-step creep tests intended to simulate fuel cell conditions in the sub-yield regime was shown to be independent of the cycle frequency. In contrast, the total strain was primarily controlled by the duration of the creep stress, revealing significant accumulation of permanent deformation even below the yield point, which may pose a concern for fuel cell operation. Overall, the present analysis revealed the critical role of the catalyst layers in determining the creep deformation of the membrane under relevant fuel cell conditions and further provided

a benchmark to improve the fundamental understanding of the creep response of fuel cell materials, which is important in the context of durability.

Acknowledgments

The authors gratefully acknowledge Automotive Partnership Canada (APC), Ballard Power Systems, and the Natural Sciences and Engineering Research Council (NSERC) for supporting this project. Ballard Power Systems is also acknowledged for providing material samples. We thank 4D LABS and the Integrated Multi-Transducer Systems Lab at Simon Fraser University as well as Spencer Arbour, Chan Lim, and Zachary Nunn for their technical support.

References

[1] C.S. Gittleman, F.D. Coms, Y. Lai, in: M.M. Mench, E.C. Kumbur, T.N. Veziroglu (Eds.), Polymer Electrolyte Fuel Cell Degradation, Elsevier Inc., 2012, pp. 15–88.
[2] L. Eudy, K. Chandler, C. Gikakis, Fuel Cell Buses in U.S. Transit Fleets: Current Status 2012, 2012.
[3] Fuel Cell Technical Team Roadmap Hydrogen Storage Technologies Roadmap, 2013.
[4] F.D. Coms, ECS Trans. 16 (2008) 235.
[5] S. Zhang, X. Yuan, H. Wang, W. Merida, H. Zhu, J. Shen, S. Wu, J. Zhang, Int. J. Hydrog. Energ. 34 (2009) 388.
[6] A. Collier, H. Wang, X. Zi Yuan, J. Zhang, D.P. Wilkinson, Int. J. Hydrog. Energ. 31 (2006) 1838.
[7] M.P. Rodgers, L.J. Bonville, H. Russell Kunz, D.K. Slattery, J.M. Fenton, Am. Chem. Soc. 112 (2012) 6075.
[8] H. Tang, S. Peikang, S.P. Jiang, F. Wang, M. Pan, J. Power Sources 170 (2007) 85.
[9] F. Bauer, S. Denneler, M. Willert-Porada, J. Polym. Sci. Pol. Phys. 43 (2005) 786.
[10] J.T. Hinatsu, M. Mizuhata, H. Takenaka, J. Electrochem Soc. 141 (1994) 1493.
[11] Y. Tang, A.M. Karlsson, M.H. Santare, M. Gilbert, S. Cleghorn, W.B. Johnson, Mat. Sci. Eng. A 425 (2006) 297.
[12] S. Kundu, L.C. Simon, M. Fowler, S. Grot, Polymer 46 (2005) 11707.
[13] M.F. Mathias, R. Makharia, H.A. Gasteiger, J.J. Conley, T.J. Fuller, C.J. Gittleman, S.S. Kocha, D.P. Miller, C.K. Mittelsteadt, T. Xie, S.G. Yan, P.T. Yu, U.S.H. Hoover, Electrochem Soc. Interface (2005) 24.
[14] M.A. Goulet, R.M.H. Khorasany, C. De Torres, M. Lauritzen, E. Kjeang, G.G. Wang, N. Rajapakse, J. Power Sources 234 (2013) 38.
[15] R.M.H. Khorasany, M.A. Goulet, A.S. Alavijeh, E. Kjeang, G.G. Wang, R.K.N.D. Rajapakse, J. Power Sources 252 (2014) 176.
[16] M.A. Goulet, S. Arbour, M. Lauritzen, E. Kjeang, J. Power Sources 274 (2015) 94.
[17] A. Wineman, K. Rajagopal, Mechanical Response of Polymers, first ed., Cambridge University Press, 2000.
[18] J. Pelleg, Mechanical Properties of Materials, Springer Netherlands, Dordrecht, 2013.
[19] R.D. Maksimov, E.A. Sokolov, V.P. Mochalov, Plenum Publishing Corporation (1976) 334.
[20] R. Scaffaro, N. Tzankova Dintcheva, F.P. La Mantia, Polym. Test. 27 (2008) 49.
[21] A. Launay, Y. Marco, M.H. Maitournam, I. Raoult, Mech. Mater. 56 (2013) 1.
[22] C.A. Tweedie, K.J. Van Vliet, J. Mater. Res. 21 (2006) 1576.
[23] H. Lu, B. Wang, J. Ma, G. Huang, H. Viswanathan, Mech. Time-Depend Mater. 7 (2003) 189.
[24] F. Achereiner, K. Engelsing, M. Bastian, P. Heidemeyer, Polym. Test. 32 (2013) 447.
[25] W. Yoon, X. Huang, J. Power Sources 196 (2011) 3933.
[26] R.M.H. Khorasany, A. Sadeghi Alavijeh, E. Kjeang, G.G. Wang, R.K.N.D. Rajapakse, J. Power Sources 274 (2015) 1208.
[27] J. Betten, Creep Mechanics, Springer-Verlag, Berlin/Heidelberg, 2005.
[28] R. Solasi, X. Huang, K. Reifsnider, Mech. Mater. 42 (2010) 678.
[29] P. Majsztrik, A. Bocarsly, J.B. Benziger, Macromolecules 41 (2008) 9849.
[30] M.B. Satterfield, P.W. Majsztrik, H. Ota, J.B. Benziger, A.B. Bocarsly, J. Polym. Sci. Pol. Phys. 44 (2006) 2327.
[31] Y. Li, D.A. Dillard, S.W. Case, M.W. Ellis, Y.H. Lai, C.S. Gittleman, D.P. Miller, J. Power Sources 194 (2009) 873.
[32] ASTM D2990-09, Standard Test Methods for Tensile, Compressive, and Flexural Creep and Creep- Rupture of Plastics, 2013, 1.